Magnetoplasmons in nondegenerate quantum wires on suspended helium films

Antonio Carlos A. Ramos,[1] O. G. Balev,[1,2] and Nelson Studart[1]
[1]*Departamento de Física, Universidade Federal de São Carlos, 13565-905, São Carlos, São Paulo, Brazil*
[2]*Institute of Semiconductor Physics, National Academy of Sciences, 45 Pr. Nauky, Kiev 252650, Ukraine*
(Received 16 October 2003; published 23 July 2004)

Magnetoplasmon spectra for the nondegenerate surface electrons confined in a quasi-one-dimensional channel over a liquid helium film are determined within a microscopic approach in the limit of strong magnetic fields when the electrons occupy the lowest spin-split Landau level. It is shown that the dispersion relation and the spatial structure, transverse to the channel, of the magnetoplasmons have a length scale $\ell_T=\sqrt{2T/m\Omega^2} \gg \ell_0$, where Ω is the confining frequency and ℓ_0 is the magnetic length. We find acoustic modes, whose velocities as a function of the gate distance exhibit a highly nonlinear behavior under certain conditions, in particular, the appearance of anticrossings.

DOI: 10.1103/PhysRevB.70.035414 PACS number(s): 73.20.Mf, 73.20.At

I. INTRODUCTION

Electrons trapped in quantum surface states deposited over the surface of a liquid helium or other cryogenic substrates have been extensively studied both theoretically and experimentally for the last 30 years.[1] The quantum confinement along the *z* direction perpendicular to the surface due to a combination of the attractive liquid polarization potential and a repulsive barrier coming from the Pauli exclusion principle leads to the formation of electron subbands analogous to the electron system in semiconductor heterostructures.[2] At low temperatures, the electrons are frozen out in the lowest state of the potential well floating more or less freely over the surface. The resulting two-dimensional electron system (2DES) can be considered as nondegenerate (N2DES) because the Fermi energy is much less the thermal energy at electron densities attainable experimentally.

Special attention has been given in understanding many-body properties of the N2DES motivated initially by the experimental investigation of the 2D plasmon dispersion and damping.[3] Afterwards the observation of edge magnetoplasmons (EMPs) constituted another intriguing and unexpected discovery in the N2DES.[4,5] EMPs are chiral collective modes that only propagate within a narrow strip very close to the boundary of the electron sheet. The important properties of the EMPs are: (i) a gapless spectrum in contrast with the usual bulk magnetoplasmon; and (ii) their frequency diminishes with increasing magnetic field. The theories of EMPs in a N2DES were developed initially (as well as for the degenerate "compressible" 2DES) within classical hydrodynamic models.[6–13] In particular, Aleiner and Glazman[12] demonstrated for a strong magnetic field *B* the existence of low-energy and long-wavelength acoustical excitations in addition to the fundamental EMP with frequency $\omega(q) \propto q\ln(1/q)$ where *q* is the one-dimensional (1D) wave vector. The existence of new patterns for EMP charge distributions is a general characteristic of the nonhomogeneous 2DES subjected to a magnetic field with a finite region where the equilibrium density profile varies. These new edge excitations have been studied experimentally in Ref. 14 for the N2DES on the helium surface.

In order to further reduce the degree of freedom of the surface electrons, a structured substrate (V-shaped, rectangular stripes, bent foil, etc.) should be introduced to restrict the electron motion to a narrow channel forming a nondegenerate quasi-one-dimensional electron system (NQ1DES).[15] The NQ1DES was also created by suspending a helium film between metallic ribs which are also used as measuring electrodes for probing a single isolated electron wire in the channel.[16] In Ref. 16, the authors observed resonances in the measured current along the channel as a function of the magnetic field which were attributed to low-frequency magnetoplasmon excitations of the NQ1DES. Recently microelectronic devices confining the electrons in microchannels have been fabricated[17] which constitute potential tools for the realization of quantum computing with electrons floating on liquid helium, as suggested by Platzman and Dykman.[18]

Previous microscopic study on the long wavelength fundamental magnetoplasmon excitation of the NQ1DES, laterally confined by a parabolic potential, somehow analogous to the fundamental EMP, showed that the spectrum has the following form:[19]

$$\omega^2(q) = \frac{2e^2}{ma} q^2 \frac{\Omega^2}{\Omega^2+\omega_c^2} \ln\frac{1}{|q\ell|}, \tag{1}$$

where $\ell^2=\hbar/m(\Omega^2+\omega_c^2)^{1/2}$, $\omega_c=|e|\,B/mc$, and Ω are the cyclotron and confinement frequencies, and $a=L/n_s$ is the mean distance between electrons in the wire of length *L* with n_s being the 2D electron density. Equation (1) is valid for values of *B* satisfying the condition $\omega_c<\Omega$. It is worthwhile to point out that the dispersion of the Q1D magnetoplasmon, given by Eq. (1), has the same form $\omega(q)\propto q\sqrt{\ln(1/q)}$ as the fundamental magnetoplasmon mode of "classical" narrow channels in the long wavelength limit.[7,13]

Inspired by the observed Q1D magnetoplasmon spectra,[16] we investigate in this paper the collective-mode excitations of the NQ1DES over a suspended liquid-helium film, with thickness d_{He}, deposited over a solid substrate with dielectric constant ϵ_s in the presence of a strong magnetic field in the direction perpendicular to the surface. At a distance *d* below the suspended-film structure, a gate electrode is inserted and

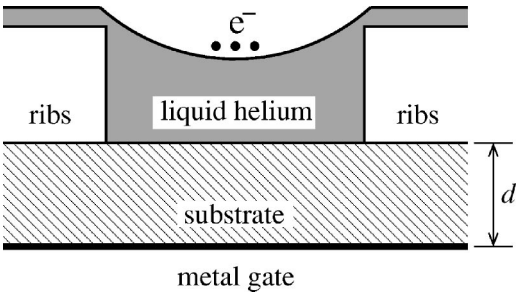

FIG. 1. Schematic drawing of the structure from Ref. 16.

the gate potential determines the holding electric field in the z direction and the electron density in the channel. A diagram of the experimental apparatus is shown in Fig. 1.

The confinement of the NQ1DES in the channel is modeled by a simple parabolic potential. Our choice is dictated by the fact that the corresponding single-particle problem can be solved analytically and, more importantly, because a self-consistent calculation of the surface profile, taking into account the effects of the van der Walls interaction of the helium film, leads approximately to an electron potential parabolic at the center of the channel for the experimental conditions of Ref. 16. We study the magnetoplasmon modes in the yet unexplored regime of strong magnetic fields, $\omega_c/\Omega \gg 1$, and in the ultraquantum limit when only the lowest spin-split Landau level is occupied, in particular, $\hbar\omega_c \gg T$.

For evaluation of the spectra and the spatial structure of the magnetoplasmons, we employ an approach, based on the random-phase approximation (RPA), developed in Ref. 20. The work presented in this paper is therefore a direct extension of the EMP problem for the 2DES in the regime of the integer quantum Hall effect to the Q1D magnetoplasmon of the NQ1DES. However, the generalization is nontrivial because, as we show, a length scale $\ell_T = \sqrt{2T/m\Omega^2} \gg \ell_0$, where $\ell_0 = (\hbar/m\omega_c)^{1/2}$ is the magnetic length, is introduced due to the fact that the electron density profile of the equilibrium NQ1DES in the parabolic channel is given by $n_0(y) = n_s^0 \exp(-y^2/\ell_T^2)$, where n_s^0 is the 2D electron density at the center of the channel.

In this paper we derive a full formula for the nonuniform electron charge densities within the RPA and solve numerically with high accuracy the corresponding eigenvalue problem to obtain the dispersion relations and charge distributions of the Q1D low-energy ($\omega \ll \omega_c$) magnetoplasmons. In particular, in the long wavelength limit $q\ell_T \ll 1$, we reproduce the usual spectrum for the fundamental mode in the absence of the bottom metal gate $\omega_0 \sim q\sqrt{\ln(1/q)}$. We obtain exactly a rich spectrum of excited acoustical modes, $\omega_j = u_j q$, with $j = 1, 2, 3, \ldots$. We also provide a detailed study of the influence of the gate on the behavior of the mode velocities u_j of the fundamental ($j=0$) and excited Q1D magnetoplasmon modes. One main result of our work is the highly nonlinear dependences of the mode velocities as a function of the gate distance that could be observed in measurements on the NQ1DES similar to those performed in the degenerate 2DES in the quantum Hall regime.[21–24] We find anticrossings in the mode velocity dependence on the gate distance.

The paper is organized as follows. In Sec. II we obtain the single-electron eigenstates in a parabolic confinement potential with a perpendicular magnetic field and we discuss the basic assumptions of our model system. In Sec. III we describe the theoretical formalism with the self-consistent approach of the RPA to obtain the equation for the electron charge density. The eigenvalue problem is solved in Sec. IV where we present and discuss the results for the spectra and charge amplitudes of the Q1D magnetoplasmon excitations. In Sec. V we give a brief summary of our work.

II. NONINTERACTING SURFACE ELECTRONS IN THE CHANNEL

We consider a parabolic confinement potential in the y direction, $V(y) = m\Omega^2 y^2/2$ where Ω is the confinement frequency depending on the holding field and on other parameters related to the substrate structure. We also assume that $V(y)$ is smooth on the scale of ℓ_0 such that $\Omega \ll \omega_c$. In order to take advantage of the translational invariance along the channel (x axis) we choose the Landau gauge for the vector potential $\mathbf{A} = (-By, 0, 0)$. The noninteracting single electron Hamiltonian is thus given by

$$\hat{h}^0 = \left[(\hat{p}_x + eBy/c)^2 + \hat{p}_y^2\right]/2m + V(y), \tag{2}$$

where $\hat{\mathbf{p}}$ is the momentum operator. For strong magnetic fields, the eigenvalues and eigenfunctions of the noninteracting NQ1DES are well approximated by

$$E_N(k) = (N + 1/2)\,\hbar\omega_c + m\Omega^2 y_0^2/2 \tag{3}$$

and

$$\psi_\alpha(\mathbf{r}) = \exp(ikx)\Psi_N(y - y_0)/\sqrt{L}, \tag{4}$$

where $y_0 \equiv y_0(k) \approx \ell_0^2 k$. Here $\mathbf{r} = \{x, y\}$, $\alpha \equiv \{N, k\}$, where k is the 1D wave vector along the channel, and $\Psi_N(y)$ is the 1D harmonic oscillator function with the characteristic length ℓ_0. From the energy spectrum given by Eq. (3), we define the group velocity of the $\{N, k\}$ state of the Nth LL as $v_{gN}(k) = \partial E_N(k)/\hbar\,\partial k = m\Omega^2\ell_0^4 k/\hbar$. We point out that for the NQ1DES in a liquid helium based structure, at $\hbar\omega_c \gg T$, the spin-splitting of the LLs $g_0\mu_B B = \hbar\omega_c$, where g_0 is the Landé g factor and μ_B is the Bohr magneton. Because we consider that only the lowest spin-split LL is essentially occupied, the spin indices can be omitted to simplify the notation.

In the absence of interactions, the one-electron density matrix of the NQ1DES is $\langle\alpha|\hat{\rho}^{(0)}|\beta\rangle = f_\alpha\delta_{\alpha\beta}$ where $f_\alpha = \exp[-(E_\alpha - E_F)/T]$ is the Boltzmann distribution function and E_F is the Fermi energy.

III. THEORETICAL APPROACH

Within the self-consistent field version of the RPA,[25] the one-electron Hamiltonian $\hat{H}(t) = \hat{h}^0 + V(x, y, t)$ in the presence of a self-consistent potential wave $V(x, y, t) = V(\varpi, q, y)\exp[-i(\varpi t - qx)] + \text{c.c.}$ The corresponding equation of motion for the one-electron density matrix $\hat{\rho}$ reads as

$$i\hbar\frac{\partial\hat{\rho}}{\partial t}=\left[\hat{H}(t),\hat{\rho}\right]-\frac{i\hbar}{\tau}(\hat{\rho}-\hat{\rho}^{(0)}), \tag{5}$$

where the brackets denote the commutator and the final phenomenological term describes the relaxation of the perturbed $\hat{\rho}$ to its equilibrium value $\hat{\rho}^{(0)}$ Equation (5) can be solved[20] by looking for a solution $R_{\alpha\beta}(\omega)=\langle\alpha|\int_0^\infty e^{i\omega t}\hat{\rho}dt|\beta\rangle$ in power series of V as $R_{\alpha\beta}(\omega)=\Sigma_{N=0}^{\infty}R_{\alpha\beta}^{(N)}(\omega)$, where $R_{\alpha\beta}^{(0)}(\omega)=(if_\alpha/\omega)\,\delta_{\alpha\beta}$. In the regime of linear response, we consider only the first two terms of the series expansion and, by calculating $\mathrm{tr}\{\hat{\rho}[e\delta(\mathbf{r}-\hat{\mathbf{r}})]\}$, we arrive at an integral expression of the charge density wave

$$\rho(x,y,t)=\frac{e}{2\pi}\int_{-\infty+i\eta}^{\infty+i\eta}d\omega e^{-i\omega t}\sum_{\alpha\beta}R_{\alpha\beta}^{(1)}(\omega)\,\psi_\beta^*(\mathbf{r})\,\psi_\alpha(\mathbf{r}), \tag{6}$$

where

$$R_{\alpha\beta}^{(1)}(\omega)=\frac{i(f_\beta-f_\alpha)\langle\alpha|V(\varpi,q,y)\,e^{iqx}|\beta\rangle}{(\omega-\varpi)(E_\beta-E_\alpha+\hbar\omega+i\hbar/\tau)}. \tag{7}$$

From Eqs. (6) and (7) it follows that $\rho(x,y,t)=\rho(q,y,t)\exp(iqx)$. Moreover, for $t/\tau\gg1$, since the contributions related to transitional processes are already negligible we have $\rho(x,y,t)=\rho(\varpi,q,y)\exp(-i\varpi t)$. Furthermore, from Poisson's equation the potential wave $\phi(q,y,t)$ induced by $\rho(q,y,t)$ is given by

$$\phi(q,y,t)=\frac{2}{\epsilon}\int_{-\infty}^{\infty}dy'\tilde{K}_0(|q||y-y'|)\,\rho(q,y',t), \tag{8}$$

where $\epsilon=(\epsilon_s+1)/2$ and

$$\tilde{K}_0(|q|\,|y-y'|)=\sum_{p=0}^{\infty}(-1)^{p+1}\left(\frac{\epsilon_s-1}{\epsilon_s+1}\right)^p\times\left\{K_0\left[|q|\sqrt{(y-y')^2+4(p+1)^2d^2}\right]-K_0\left[|q|\sqrt{(y-y')^2+4p^2d^2}\right]\right\}, \tag{9}$$

with $K_0(x)$ being the modified Bessel function and the typical condition $d_{\mathrm{He}}\ll1/(2\sqrt{q^2+\ell_T^{-2}})$ is well satisfied. We can see that the right-hand side of Eq. (9) is well approximated by the $p=0$ term, when $(\epsilon_s-1)\ll1$ or $\exp[-2d(q_x^2+\ell_T^{-2})^{1/2}]\ll1$.

The relation $\rho(q,y,t)=\rho(q,y,\varpi)\exp(-i\varpi t)$ holds for $t\gg\tau$ and it follows from Eq. (8) that $\phi(q,y)=\phi(q,y,\varpi)\exp(-i\varpi t)$. In the absence of an external potential, we have $V(q,y,\varpi)=e\phi(q,y,\varpi)$. As a consequence from Eqs. (6), (7), and (8), the integral equation for $\rho(q,y,\omega)$ can be written as

$$\rho(q,y,\omega)=\frac{2e^2}{\epsilon L}\sum_{N_\alpha,N_\beta=0}^{\infty}\sum_{k_\alpha}\frac{f_\beta-f_\alpha}{E_\beta-E_\alpha+\hbar\omega+i\hbar/\tau}\times\Pi_{N_\alpha N_\beta}(y,k_\alpha,k_\beta)\times\int_{-\infty}^{\infty}d\tilde{y}\int_{-\infty}^{\infty}dy'\,\Pi_{N_\alpha N_\beta}(\tilde{y},k_\alpha,k_\beta)\times\tilde{K}_0(|q|\,|\tilde{y}-y'|)\rho(q,y',\omega), \tag{10}$$

where $\Pi_{N_\alpha N_\beta}(y,k_\alpha,k_\beta)=\Psi_{N_\alpha}(y-y_{0\alpha})\Psi_{N_\beta}(y-y_{0\beta})$, with $y_{0\alpha}=y_0(k_\alpha)$ and $k_\beta=k_\alpha-q$, and we set $\varpi=\omega$. An analysis of the summation over N_α and N_β in Eq. (10) indicates that the terms with $N_\alpha\neq N_\beta$ can be neglected for $\omega\ll\omega_c$ and $qv_g\ll\omega_c$. This leads to the integral equation

$$\rho(q,y,\omega)=\frac{2e^2}{\epsilon L}\sum_{N_\alpha=0}^{\bar{N}}\sum_{k_\alpha}\frac{f_{N_\alpha,k_\alpha-q}-f_{N_\alpha,k_\alpha}}{E_{N_\alpha,k_\alpha-q}-E_{N_\alpha,k_\alpha}+\hbar\omega+i\hbar/\tau}\times\Pi_{N_\alpha N_\alpha}(y,k_\alpha,k_\alpha-q)\times\int_{-\infty}^{\infty}d\tilde{y}\int_{-\infty}^{\infty}dy'\,\Pi_{N_\alpha N_\alpha}(\tilde{y},k_\alpha,k_\alpha-q)\times\tilde{K}_0(|q||\tilde{y}-y'|)\,\rho(q,y',\omega), \tag{11}$$

where $\bar{N}$ denotes the highest occupied LL. Because the strong quantizing magnetic field, $\hbar\omega_c\gg T$, the Fermi level does not cross the lowest spin-split LL and all electrons occupy only the lowest LL. Hence, $\bar{N}=0$ and Eq. (11) becomes

$$\rho(q,y,\omega)=\frac{e^2}{\pi\hbar\epsilon}\int_{-\infty}^{\infty}dk\frac{f_{0,k-q}-f_{0,k}}{\tilde{\omega}-v_{g0}(k)q}\Pi_{00}(y,k,k-q)\times\int_{-\infty}^{\infty}d\tilde{y}\int_{-\infty}^{\infty}dy'\Pi_{00}(\tilde{y},k,k-q)\times\tilde{K}_0(|q||\tilde{y}-y'|)\rho(q,y',\omega), \tag{12}$$

where $\tilde{\omega}=\omega+i/\tau$. Assuming that $q\ell_0\ll1$, then $\Pi_{00}(y,k,k-q)\approx\Pi_{00}(y,k,k)$ with $\Pi_{00}(y,k,k)=\exp[-(y-y_0)^2/\ell_0^2]/\sqrt{\pi}\ell_0$. Using this expression in Eq. (12) we obtain

$$\rho(q,y,\omega)=\frac{e^2}{\pi^2\hbar\epsilon\ell_0^2}\int_{-\infty}^{\infty}dk\frac{f_{0,k-q}-f_{0,k}}{\tilde{\omega}-v_{g0}(k)q}e^{-(y-y_0)^2/\ell_0^2}\times\int_{-\infty}^{\infty}d\tilde{y}\int_{-\infty}^{\infty}dy'e^{-(\tilde{y}-y_0)^2/\ell_0^2}\times\tilde{K}_0(|q||\tilde{y}-y'|)\,\rho(q,y',\omega), \tag{13}$$

where $f_{0,k}=\nu\exp(-\ell_0^4k^2/\ell_T^2)$ and $\nu=\exp[(E_F-\hbar\omega_c/2)/T]=2\pi\ell_0^2n_s^0$ is the filling factor in the center of the channel. Obviously $\nu\ll1$ in the present case. For $q\ell_0\ll1$ it follows that:

$$f_{0,k-q}-f_{0,k}\approx\frac{2\nu\ell_0^4kq}{\ell_T^2}e^{-\ell_0^4k^2/\ell_T^2}, \tag{14}$$

which is valid if $\ell_0^2/\ell_T^2\lesssim1$. Using Eq. (14) into Eq. (13) we obtain

$$\rho(q,y,\omega) = \frac{4e^2 n_s^0 q}{\pi\hbar\epsilon\ell_T^2}\int_{-\infty}^{\infty} dy_0 \frac{y_0 \exp(-y_0^2/\ell_T^2)}{\tilde{\omega} - v_{g0}(y_0/\ell_0^2)q} e^{-(y-y_0)^2/\ell_0^2} \times \int_{-\infty}^{\infty} d\tilde{y} \int_{-\infty}^{\infty} dy' e^{-(\tilde{y}-y_0)^2/\ell_0^2} \times \tilde{K}_0(|q||\tilde{y}-y'|)\,\rho(q,y',\omega). \quad (15)$$

Furthermore, since $\ell_T \gg \ell_0$, we can approximate $\exp[-(x-y_0)^2/\ell_0^2]$ by $\sqrt{\pi}\ell_0\delta(x-y_0)$. After integration, it follows that:

$$[\tilde{\omega} - CqH_1(y/\ell_T)]\,\rho(q,y,\omega) = QqH_1(y/\ell_T)\,\psi_0^2(y/\ell_T) \times \int_{-\infty}^{\infty} dy' \tilde{K}_0(|q||y-y'|)\,\rho(q,y',\omega), \quad (16)$$

where $C=\Omega^2\ell_T/2\omega_c$, $Q=2\sqrt{\pi}|e|cn_s^0/\epsilon B$, we used that $v_{g0}(y/\ell_0^2)=\Omega^2 y/\omega_c$ and $H_n(x)$ is the Hermite polynomial. From Eq. (16) we see that its nontrivial solutions are neither symmetric, $\rho_s(q,-y,\omega)=\rho_s(q,y,\omega)$, nor antisymmetric, $\rho_a(q,-y,\omega)=-\rho_a(q,y,\omega)$. In other words, we want to underline that the solutions will not have a definite parity. We will seek a solution of Eq. (16) in the form

$$\rho(q,y,\omega) = H_1(y/\ell_T)\psi_0^2(y/\ell_T)\sum_{n=0}^{\infty}\rho^{(n)}(q,\omega)\,H_n(y/\ell_T), \quad (17)$$

which is an exact expansion due to the orthogonality of the $H_n(x)$. We point out that the even (odd) terms in Eq. (17) give purely antisymmetric (symmetric) contributions to $\rho(q,y,\omega)$. Then the mixture of both symmetric and antisymmetric terms should be present in Eq. (17) to have a nontrivial solution. In particular, we need take at least the first two terms, $n=0,1$, to obtain the fundamental magnetoplasmon mode. Substituting Eq. (17) in Eq. (16) then multiplying Eq. (16) by $H_m(y/\ell_T)/H_1(y/\ell_T)$ and integrating over y, we obtain for $\rho^{(m)}(q,\omega)$:

$$\tilde{\omega}\rho^{(m)}(\omega) - Cq[\rho^{(m-1)}(\omega) + 2(m+1)\,\rho^{(m+1)}(\omega)] = \frac{Qq}{2^m m!}\sum_{n=0}^{\infty}\rho^{(n)}(\omega)I_{mn}(q), \quad (18)$$

with

$$I_{mn}(q) = \frac{1}{\pi}\int_{-\infty}^{\infty}\int_{-\infty}^{\infty} dY dY' H_m(Y)\exp[-(Y^2+Y'^2)] \times \tilde{K}_0(|q|\ell_T|Y-Y'|)H_1(Y')H_n(Y'), \quad (19)$$

where $Y=y/\ell_T$. Observe that $I_{mn}(q)\equiv 0$ if $(m+n)$ is an even number. We emphasize that the parameter C is related to one-particle confinement effects, i.e., advection contributions related with the energy dispersion of the LL while Q corresponds to contributions from electron-electron interactions.

IV. RESULTS AND DISCUSSION

In this section, we present our results for the dispersion relations and spatial structures of magnetoplasmons in the NQ1DES obtained through the solution of Eq. (18) for a wide range of $q\ell_T$. We neglect the dissipation by assuming $\tau\to\infty$, and as a consequence $\tilde{\omega}=\omega$. Considering the terms $n,m=0,1$ in Eqs. (18) and (17) we obtain

$$\omega\rho^{(0)}(q,\omega) - q[2C + QI_{01}(q)]\rho^{(1)}(q,\omega) = 0, \quad (20)$$

and

$$q\left[C + \frac{Q}{2}I_{10}(q)\right]\rho^{(0)}(q,\omega) - \omega\rho^{(1)}(q,\omega) = 0. \quad (21)$$

From Eqs. (20) and (21), the dispersion relation for the fundamental magnetoplasmon mode can be written as

$$\omega_0^2 = q^2\left\{2C^2 + CQ[I_{10}(q)+I_{01}(q)] + \frac{Q^2}{2}I_{10}(q)I_{01}(q)\right\}, \quad (22)$$

with positive (ω_+) and negative (ω_-) modes propagating forth and back along the x axis. In the absence of the metallic gate ($d\to\infty$) and in the long wavelength limit ($q\ell_T\ll 1$) we obtain, from Eq. (22), the dispersion relation for the fundamental plasmon mode of the NQ1DES as

$$\omega_{0\pm} = \pm\frac{2\sqrt{\pi}|e|cn_s^0}{\epsilon B}q\left[\ln\left(\frac{2}{q\ell_T}\right) - 0.44\right]^{1/2}, \quad (23)$$

which is close to the fundamental magnetoplasmon dispersion obtained in previous works.[13,19] As we consider a finite d, we find the interesting result that the fundamental mode is acoustical in the long wavelength limit for $d/\ell_T \lesssim 1$. In addition, for $d/\ell_T \ll 1$, it follows from Eq. (22) that the mode velocity $u_0=\omega_0/q$ is given by

$$u_0 = \frac{\Omega^2\ell_T}{\sqrt{2}\omega_c} + \frac{2\pi|e|cn_s^0}{\epsilon_s B}\frac{d}{\ell_T}. \quad (24)$$

We now go further by considering terms up to $n,m=9$ in Eqs. (17) and (18). In this case, the dispersion relation is obtained in terms of a fifth-degree polynomial for ω^2 which yields five magnetoplasmon modes propagating in each direction of the x axis. Two of them correspond to the fundamental magnetoplasmon modes $\omega_{0\pm}$ determined with accurate precision for all $q\ell_T$. If otherwise not stated, we present the results for the ω_+ modes, assuming $q>0$ and $\omega_+>0$.

In Fig. 2, the fundamental magnetoplasmon frequency is depicted as a function of $(q\ell_T)^{-1}$ for a choice of parameters similar to the experimental values in Ref. 16: $n_s=2\times10^8$ cm^{-2}, $\epsilon=3$, $\Omega=10^8$ s^{-1}, $T=0.6$ K, and $B=3.6$ T, which correspond to $\hbar\omega_c=0.42$ meV, $\omega_c/\Omega\approx 6.3\times10^3$, $\ell_T=42.6$ μm, and $\ell_T/\ell_0\approx 3.2\times10^3$. The characteristic frequency $\omega_*=2\sqrt{\pi}|e|cn_s^0/\epsilon\ell_T B\approx 2.2\times10^7$ s^{-1}. The solid, dashed, and dotted curves in Fig. 2 are for $d\to\infty, 10^{-2}$ and 10^{-3} cm, from top to bottom, respectively. We note from the inset of Fig. 2, where the mode velocity u in units of u_*

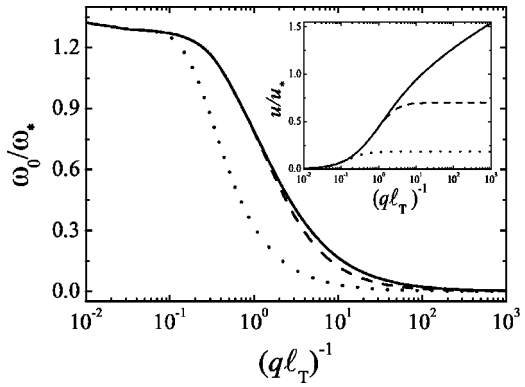

FIG. 2. Fundamental mode spectrum $\omega_0(q)$ in units of $\omega_* = 2\sqrt{\pi}|e|cn_s^0/\epsilon\ell_T B$ for the NQ1DES in the absence of gate ($d \to \infty$) indicated by the solid line and for gate distances $d = 10^{-2}$ cm (dashed line) and $d = 10^{-3}$ cm (dotted line). In the inset, the mode velocity is shown, in units of $u_* = 2\pi|e|cn_s^0/\epsilon B$. The spectrum was calculated from the 10×10 equation system in Eq. (18). The parameters are chosen to be the same as in the experiment of Ref. 16.

$= \sqrt{\pi}\omega_*\ell_T = 2\pi|e|cn_s^0/\epsilon B$ is shown, that the region of acoustical dispersion appears when $2\kappa d \ll 1$, where $\kappa = \sqrt{q^2 + q_y^2}$ and $q_y \sim \ell_T^{-1}$.

We depict in Fig. 3 the charge density amplitude $\rho(q, y, \omega)/\rho_*$, where $\rho_* = \rho^{(0)}(q, \omega)/\sqrt{\pi}\ell_T$, for the fundamental mode as a function of $Y = y/\ell_T$ for $(q\ell_T)^{-1} = 100$ and different gate distances for seeing the influence of the metal plate on the structure of the magnetoplasmon mode. The parameters are the same as for the corresponding curves in Fig. 2. In the inset, we display the amplitudes for the modes ω_{0+} (solid) and ω_{0-} (dashed) of the NQ1DES in the absence of gate, $d \to \infty$. We clearly observe the chirality of these two branches.

The dispersion relations for the first and second excited modes, described by Eq. (18), are shown in Fig. 4 for the same parameters used in Fig. 2. The first (second) excited mode is represented by the upper (lower) curve. Solid curves

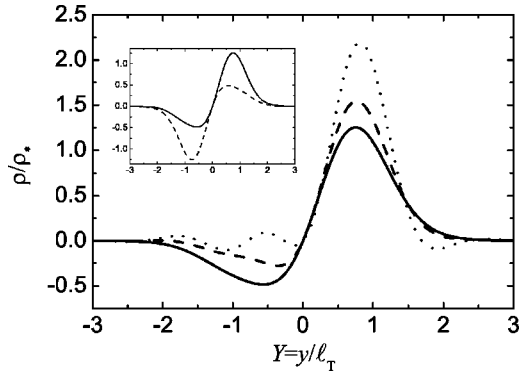

FIG. 3. Spatial structure of the fundamental mode $\rho(q, y, \omega)$, in units of $\rho_* = \rho^{(0)}(q, \omega)/\sqrt{\pi}\ell_T$, calculated from the 10×10 system, for $(q\ell_T)^{-1} = 100$. The solid, the dashed and the dotted curves parameters coincide with those of pertinent curves in Fig. 2. In the inset the solid (dashed) curve plots ρ/ρ_* for ω_{0+} (ω_{0-}) mode in the absence of gate.

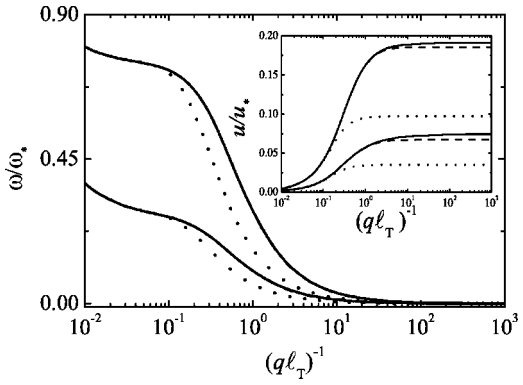

FIG. 4. Dispersion relations for the first (upper curve) and second (lower curve) excited Q1D magnetoplasmons. The solid and the dotted curves correspond to the same parameters as the pertinent curves in Fig. 2. In the inset the mode velocities are shown with the dashed curve corresponding to $d = 10^{-2}$ cm.

correspond to the modes in the structure without a metal gate, while the dotted curve corresponds to the mode in the gated structure with $d = 10^{-3}$ cm. No marked difference is found for $d = 10^{-2}$ cm. In the inset of Fig. 4 we show the mode velocity as a function of $(q\ell_T)^{-1}$. Now we observe a slight deviation when $d = 10^{-2}$ cm represented by the dashed line. The screening effect from the bottom plate is stronger on the first excited mode and the overall influence of the gate is to diminish the frequencies of all modes. As expected the spectrum exhibits only low-lying excitation modes which are acoustical for $q \ll 1/\sqrt{\ell_T^2 + 4d^2}$.

We show in Fig. 5, the influence of the temperature on the dispersion of the magnetoplasmon modes in the NQ1DES without the gate for $T = 0.4$ K (solid curve) and 1 K (dashed curve) and the same conditions of Fig. 2. The fundamental and the first and second excited modes are indicated by the top, middle, and bottom curves, respectively. As we can see the differences appear only for $q\ell_T > 10$ and are due to the advection contribution in Eq. (18).

In Fig. 6 the spatial structure of the charge density is depicted for the first two excited modes of the NQ1DES

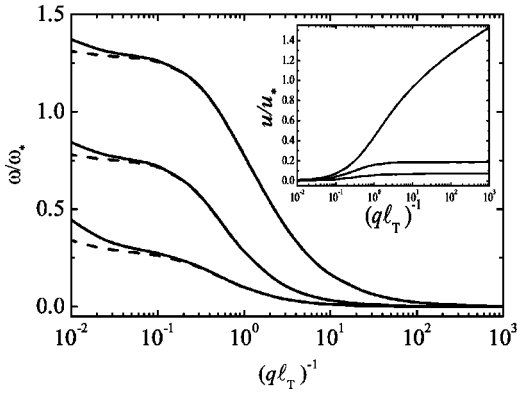

FIG. 5. Dispersion relation for the fundamental (top curve) and two excited magnetoplasmons (curves below) for the structure without the gate for $T = 1$ K (solid line) and $T = 0.4$ K (dashed line). Other parameters are the same as in Fig. 2. In the inset we show the mode velocities.

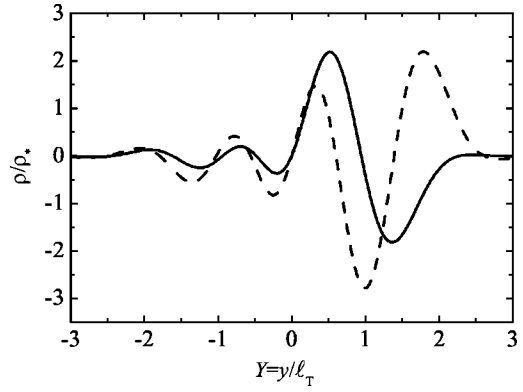

FIG. 6. Spatial structure of charge density for the first excited modes in the channel without the metallic gate calculated for $q\ell_T=0.01$. The solid (dashed) line represent the first (second) excited magnetoplasmon.

without the metallic gate for the conditions of Fig. 3. The solid and dashed curves in Fig. 6 correspond to the first and second excited positive magnetoplasmons, respectively, and are calculated for $q\ell_T=0.01$. Note that in the usual Q1D fundamental mode (solid line in Fig. 3), the charge density does not oscillate around the channel center in contrast with the excited modes.

Furthermore, in Fig. 7 we present the mode velocity versus the gate distance for the first five positive modes indicated by the solid, dashed, dotted, dot-dashed, and dot-dot-dashed curves. We observe that the mode velocities exhibit anti-crossings at $d/\ell_T \ll 1$. All anticrossings have a finite gap, even though some of them are very small in that scale. In the inset of Fig. 7, the velocities for these five modes are shown twofold: (i) by five solid curves, when the second term in the left-hand side of Eq. (18) is neglected; and (ii) by five dashed curves, if the right-hand side of Eq. (18) is taken as zero. These solid curves correspond to the case when the advection contributions related with the energy dispersion of the LL are omitted (C term is neglected) while the dashed curves are evaluated when contributions due to the electron-electron

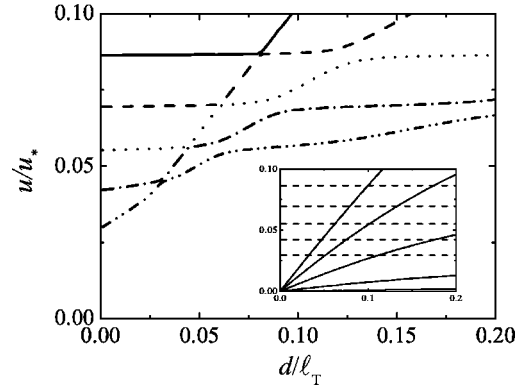

FIG. 7. Mode velocity versus gate distance for the first five modes represented by the solid, dashed, dotted, dot-dashed and dot-dot-dashed curves. In the inset these modes are indicated by five solid (dashed) curves when the C (Q) term of Eq. (18) is neglected. Here $n_s=2\times10^7$ cm^{-2}, $\Omega=5\times10^8$ cm^{-1} and the other parameters are the same as in Fig. 2.

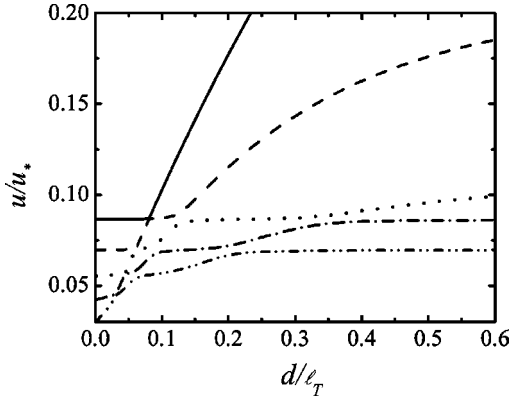

FIG. 8. Same as Fig. 7 in a wide region of d/ℓ_T. We clearly see additional anticrossings for larger d/ℓ_T.

interaction (Q term is neglected) are omitted. The parameters used in Fig. 7 are $n_s=2\times10^7$ cm^{-2}, $\epsilon=3$, $\Omega=5\times10^8$ s^{-1}, $T=0.6$, and $B=3.6$ T giving now $u_*\approx1.68\times10^4$ cm/s. For better accuracy of the results, we have also checked out all crossings and anticrossings shown in Fig. 7 by solving the determinantal equation up to $n,m=19$ in Eqs. (17) and (18), which gives the dispersion relation as a tenth-degree polynomial for ω^2.

In Fig. 8 we plot the mode velocity for a wider region of d/ℓ_T. There are two anticrossings beyond those shown in Fig. 7, at $d/\ell_T>0.2$. It is seen in Figs. 7 and 8 that the mode velocities of all magnetoplasmon modes show nonlinear behavior as a function of d/ℓ_T as for $d/\ell_T\lesssim1$ as well for $d/\ell_T\ll1$. It is essentially different from the result of Ref. 24 where $u\propto d/\ell$, for $d/\ell\to0$, in the compressible region of the width ℓ at the edge of the degenerate 2DES in the quantum Hall regime. From the two terms appearing in Eq. (24), we observe that $u\propto d/\ell_T$, similar to the result of Ref. 24, only when $d\gg d_a$, where $d_a=T\epsilon_s/(\sqrt{2}\pi e^2 n_s^0)$. Because the condition $e^2/\epsilon_s\ell_0\gg T$ is well satisfied in the NDQ1DES, the necessary condition for the appearance of the anticrossing region, $d\lesssim d_a$, as shown in Figs. 7 and 8, $d_a/\ell_0\gg1$ implies that $\nu\ll1$. The latter is in agreement with assumptions of our model.

V. SUMMARY

We study low frequency magnetoplasmon excitations of the nondegenerate two-dimensional electron system laterally confined by a parabolic quantum well forming a quasi-one-dimensional electron system. Starting from the equation of motion for the electron density operator we employ the self-consistent method to obtain the algebraic matrix representation of the integral equation for the wave charge density in the NQ1DES. In the simplest approximation, the eigenvalue equations are reduced to only two equations and we derive the dispersion relation for the fundamental mode which is similar to the previous results obtained in the hydrodynamic method as well in the perturbation approach to the dielectric function within the random-phase approximation. We solve numerically the matrix equation with high accuracy to obtain the fundamental and excited magnetoplasmon modes for q

$\ll \ell_T^{-1}$ as well for the interesting wide region $\ell_0^{-1} \gg q \gtrsim \ell_T^{-1}$. We discuss the influence of screening due to the metal gates on the plasmon dispersion and the mode velocity. For $q \ll \ell_T^{-1}$ our results show that all excited modes are acoustical. Furthermore, for $d/\ell_T \lesssim 1$ and $q \ll \ell_T^{-1}$ the magnetoplasmon modes are acoustical and their velocities display a nontrivial dependence on the gate distance. Moreover, there are a number of anticrossings (and, in principle, infinite) within the well-defined characteristic length which are more easily achievable for $d/\ell_T \ll 1$, smaller electron density and larger confinement frequency. We show that the anticrossings are essentially connected both with the electron-electron interaction and the dispersion of the lowest Landau level, through the quantum number k. Finally, we speculate that our predicted results may be verified through time-resolved magnetotransport measurements.

ACKNOWLEDGMENTS

This work was supported in part by a grant from Fundação de Amparo à Pesquisa do Estado de São Paulo (FAPESP), A.C.A.R. acknowledges FAPESP and O.G.B. and N.S. are grateful to the Conselho Nacional de Desenvolvimento Científico e Tecnológico (CNPq).

[1] See, for instance, the review book *Two-Dimensional Electron Systems in Helium and Other Substrates*, edited by E. Y. Andrei (Kluwer, Dordrecht, 1997).
[2] T. Ando, A. B. Fowler, and F. Stern, Rev. Mod. Phys. **54**, 437 (1982).
[3] C. C. Grimes and G. Adams, Phys. Rev. Lett. **36**, 145 (1976).
[4] D. B. Mast, A. J. Dahm, and A. L. Fetter, Phys. Rev. Lett. **54**, 1706 (1985).
[5] D. C. Glattli, E. Y. Andrei, G. Deville, J. Poitrenaud, and F. Williams, Phys. Rev. Lett. **54**, 1710 (1985).
[6] V. A. Volkov and S. A. Mikhailov, Pis'ma Zh. Eksp. Teor. Fiz. **42**, 450 (1985) [JETP Lett. **42**, 556 (1985)].
[7] V. A. Volkov and S. A. Mikhailov, Zh. Eksp. Teor. Fiz. **94**, 217 (1988) [Sov. Phys. JETP **67**, 1639 (1988)].
[8] A. L. Fetter, Phys. Rev. B **32**, 7676 (1985).
[9] A. L. Fetter, Phys. Rev. B **33**, 3717 (1986); Phys. Rev. B **33**, 5221 (1986).
[10] V. Cataudella and G. Iadonisi, Phys. Rev. B **35**, 7443 (1987).
[11] S. S. Nazin and V. B. Shikin, Zh. Eksp. Teor. Fiz. **94**, 133 (1988) [Sov. Phys. JETP **67**, 288 (1988)].
[12] I. L. Aleiner and L. I. Glazman, Phys. Rev. Lett. **72**, 2935 (1994).
[13] I. L. Aleiner, D. Yue, and L. I. Glazman, Phys. Rev. B **51**, 13 467 (1995).
[14] O. I. Kirichek, P. K. H. Sommerfeld, Yu. P. Monarkha, P. J. M. Peters, Yu. Z. Kovdrya, P. P. Steijaert, R. W. van der Heijden, and A. T. A. M. de Waele, Phys. Rev. Lett. **74**, 1190 (1995).
[15] For a review, see Yu. Z. Kovdrya, Fiz. Nizk. Temp. **29**, 107 (2003) [Low Temp. Phys. 29, **77** (2003)], and references therein.
[16] A. M. C. Valkering and R. W. van der Heijden, Physica B **249-251**, 652 (1998).
[17] P. Glasson, V. Dotsenko, P. Fozooni, M. J. Lea, W. Bailey, G. Papageorgiou, S. E. Andresen, and A. Kristensen, Phys. Rev. Lett. **87**, 176802 (2001).
[18] P. M. Platzman and M. I. Dykman, Science **284**, 1967 (1999); M. I. Dykman and P. M. Platzman, Fortschr. Phys. **48**, 1095 (2000).
[19] S. S. Sokolov and N. Studart, Phys. Rev. B **57**, R704 (1998).
[20] O. G. Balev and P. Vasilopoulos, Phys. Rev. B **59**, 2807 (1999).
[21] R. C. Ashoori, H. L. Stormer, L. N. Pfeiffer, K. W. Baldwin, and K. West, Phys. Rev. B **45**, 3894 (1992).
[22] G. Ernst, R. J. Haug, J. Kuhl, K. von Klitzing, and K. Eberl, Phys. Rev. Lett. **77**, 4245 (1996).
[23] N. B. Zhitenev, R. J. Haug, K. von Klitzing, and K. Eberl, Phys. Rev. B **52**, 11 277 (1995).
[24] G. Ernst, N. B. Zhitenev, R. J. Haug, and K. von Klitzing, Physica E (Amsterdam) **1**, 95 (1997).
[25] P. M. Platzmann and P. A. Wolff, *Waves and Interactions in Solid State Plasmas*, Solid State Physics Suppl. 13, edited by H. Ehrenreich, F. Seitz, and D. Turnbull (Academic, New York, 1973).